THE JOURNAL OF BIOLOGICAL CHEMISTRY VOL. 287, NO. 52, pp. 43972–43983, December 21, 2012

Functional Analysis of Missense Mutations in Kv8.2 Causing Cone Dystrophy with Supernormal Rod Electroretinogram*

Received for publication, June 6, 2012, and in revised form, October 29, 2012 Published, JBC Papers in Press, October 31, 2012, DOI 10.1074/jbc.M112.388033

Katie E. Smith[‡§], Susan E. Wilkie[‡], Joseph T. Tebbs-Warner[§], Bradley J. Jarvis[§], Linn Gallasch[§1], Martin Stocker[§2], and David M. Hunt[‡¶3]

From the [‡]University College London Institute of Ophthalmology, London EC1V 9EL, United Kingdom, the [§]Department of Neuroscience, Physiology, and Pharmacology, University College London, London WC1E 6BT, United Kingdom, and the [¶]School of Animal Biology, Oceans Institute, and Lions Eye Institute, University of Western Australia, Perth 6009, Australia

Background: Homozygosity mapping linked mutations in *KCNV2*, encoding Kv8.2, to an inherited retinal disorder.
Results: Mutant Kv8.2 subunits render heteromeric Kv2.1/Kv8.2 channels nonfunctional or fail to form heteromers, resulting in homomeric Kv2.1 channels.
Conclusion: Although clinically indistinguishable, different missense mutations impair channel function via two distinct molecular mechanisms.
Significance: Loss of channel function arising from *KCNV2* mutations is confirmed.

Mutations in *KCNV2* have been proposed as the molecular basis for cone dystrophy with supernormal rod electroretinogram. *KCNV2* codes for the modulatory voltage-gated potassium channel α-subunit, Kv8.2, which is incapable of forming functional channels on its own. Functional heteromeric channels are however formed with Kv2.1 in heterologous expression systems, with both α-subunit genes expressed in rod and cone photoreceptors. Of the 30 mutations identified in the *KCNV2* gene, we have selected three missense mutations localized in the potassium channel pore and two missense mutations localized in the tetramerization domain for analysis. We characterized the differences between homomeric Kv2.1 and heteromeric Kv2.1/Kv8.2 channels and investigated the influence of the selected mutations on the function of heteromeric channels. We found that two pore mutations (W467G and G478R) led to the formation of nonconducting heteromeric Kv2.1/Kv8.2 channels, whereas the mutations localized in the tetramerization domain prevented heteromer generation and resulted in the formation of homomeric Kv2.1 channels only. Consequently, our study suggests the existence of two distinct molecular mechanisms involved in the disease pathology.

Cone dystrophy with supernormal rod electroretinogram (CDSRE)[4] is a progressive retinal disorder belonging to a genetically diverse group of photoreceptor dystrophies. The condition is diagnosed upon presentation of a characteristic electroretinogram (ERG) used to assess the functional integrity of the retina. Scotopic and photopic responses are reduced and delayed, indicating impairment of rod and cone photoreceptor pathways, respectively. However, at higher light intensities, scotopic b-wave responses are supernormal in amplitude (1).

CDSRE presents a recessive mode of inheritance and was recently shown to arise from mutations in *KCNV2*, the gene encoding a voltage-gated K^+ (Kv) channel α-subunit, Kv8.2 (2). There are 12 subfamilies of Kv α-subunits in humans. All share a common structure comprising six transmembrane domains (S1–S6) with cytoplasmic COOH and NH_2 termini; a voltage domain S1–S4, with regularly spaced positively charged amino acids in S4; and a pore domain, S5-pore-S6, containing the K^+ channel signature Gly-Tyr-Gly, which forms the selectivity filter. The amino-terminal tetramerization (T1) domain present in Kv1–Kv6, Kv8, and Kv9 α-subunits encodes molecular determinants for subfamily-specific assembly (3, 4).

Kv channels are composed of four α-subunits arranged around a central K^+-conducting pore (4). The T1 domain facilitates the interaction between compatible α-subunits (5, 6) while preventing the tetramerization of α-subunits containing incompatible domains (6). Kv1 to Kv4 α-subunits lacking T1 domains, however, assemble promiscuously (7).

Although the α-subunits of the Kv1–Kv6, Kv8, and Kv9 subfamilies share a common structure, only the Kv1–Kv4 α-subunits form functional homo- and heteromeric channels within their subfamilies (8–10). The T1 domain of Kv5, Kv6, Kv8, and Kv9 α-subunits prevents the formation of functional homomeric channels within these subfamilies (11–14) but enables the formation of heteromeric channels with Kv2 subunits. These heteromeric channels show some biophysical properties that differ from those of homomeric Kv2 channels (11–25).

* This work was supported in part by United Kingdom Biotechnology and Biological Sciences Research Council Grant BB/E023142/1 (to D. M. H. and M. S.) and Australian National Health and Medical Research Council Grant AP102740 (to D. M. H.).
[1] Supported by Biotechnology and Biological Sciences Research Council Doctoral Training Grant Studentship BB/D526961/1.
[2] To whom correspondence may be addressed. Tel.: 44-207-679-7244; Fax: 44-207-679-7245; E-mail: M.Stocker@ucl.ac.uk.
[3] To whom correspondence may be addressed: School of Animal Biology, Oceans Institute, and Lions Eye Institute, University of Western Australia, Perth 6009, Australia. Tel.: 61-8-6488-3044; Fax: 61-8-6488-7527; E-mail: david.hunt@uwa.edu.au.
[4] The abbreviations used are: CDSRE, cone dystrophy with supernormal rod electroretinogram; COS7L, African green monkey kidney fibroblast-like cell; EGFP, enhanced green fluorescent protein; ERG, electroretinogram; HEK293, human embryonic kidney cells; Kv, voltage-gated potassium channel; p, pulse; RIPA, radioimmunoprecipitation assay; T1 domain, tetramerization domain; TRITC, tetramethyl rhodamine isothiocyanate; ANOVA, analysis of variance; m, mouse; h, human; r, rat.

More than 30 unique mutations in *KCNV2* have been identified in patients with CDSRE (2, 26–33). These include missense, nonsense, frameshift, nonstop, and deletion mutations. The purpose of this study is to elucidate the functional outcome of several missense mutations located in different parts of the Kv8.2 α-subunit.

EXPERIMENTAL PROCEDURES

Molecular Biology—The human (h) and mouse (m) cDNAs of Kv2.1 and Kv8.2 were cloned into a modified version of pcDNA3 containing the 5′UTR of the *Xenopus* β-globin gene (construct name and GenBank™ accession number: hKv2.1 NM_004975; mKv2.1 BC031776; hKv8.2 BC101353; and mKv8.2 BC039042). Mutations were introduced into Kv8.2 with the QuikChange site-directed mutagenesis kit (Stratagene, La Jolla, CA). EGFP was fused to the COOH terminus of the indicated constructs by in-frame cloning into pEGFP-N1 (Clontech). Splicing by overlap extension was used to introduce mutations into Kv2.1 (34). All constructs were verified by sequencing.

Fluorescence Imaging—COS7L cells were cultured (in a humidified atmosphere, 5% CO_2, 95% air) at 37 °C in DMEM with high glucose, supplemented with L-glutamine, penicillin/streptomycin, and 10% FBS. For transfection, cells were cultured on 13-mm glass coverslips and transfected at low density (~30%) using 3 μl of GeneJuice (Novagen, Merck) and 1 μg of total cDNA. Kv8.2-EGFP was cotransfected with Kv2.1 in a 1:3 ratio. Cells were fixed with 4% paraformaldehyde in PBS 48 h post-transfection. For Kv2.1 antibody staining, cells were permeabilized (0.1% Triton X-100), washed, pre-blocked (5% FBS in PBS, 30 min), and then incubated for 1 h with the K89/34 antibody (1:400 in blocking solution; University of California at Davis/National Institutes of Health Neuromab Facility). After repeated washes with PBS, the cells were incubated again in blocking solution (30 min), followed by application of the secondary antibody (1:600; 1 h), and either TRITC-conjugated goat anti-mouse (Sigma) or Cy3-conjugated goat anti-mouse antibody (The Jackson Laboratory, Newmarket, UK). After further washes in PBS, the coverslips were mounted with VECTASHIELD (Vector Laboratories, Burlingame, CA). Confocal images were acquired using a Leica TCS SPE with a ×40 oil immersion objective (1.15 NA). Solid state lasers at 488 nm (EGFP) and 532 nm (TRITC) were used for excitation. Emission ranges of 500–525 nm for EGFP and 545–650 nm for TRITC were set via the spectrophotometer detection system. Sequential scanning was used to image cotransfected cells, and bleed through was not observed. Imaging for hKv2.1 and hKv2.1 mutants was performed on a Leica SP5 confocal microscope using a ×40 oil immersion objective (1.25 NA). Excitation of Cy3 was performed using an argon laser (514 nm), and emission was collected between 548 and 631 nm.

Electrophysiology—HEK293 cells were cultured in DMEM/F-12 with the same supplements and under the same conditions as for COS7L cells. Cells were transfected at 80–90% confluency with 2.5 μg of DNA using a Lipofectamine 2000 (Invitrogen) to DNA ratio of 2:1. For studies of Kv2.1/Kv8.2, 90 ng of Kv2.1-pcDNA3 was used with an equal amount of Kv8.2-pcDNA3. For studies of Kv2.1, 50 or 90 ng of Kv2.1-pcDNA3 was transfected. To visualize transfected cells, 100–150 ng of pEGFP-C2 was included together with pcDNA3 to transfect constant amounts of DNA. 18–22 h post-transfection, cells were plated on glass coverslips and allowed to recover for 3–4 h before recording. Cell recordings were performed at room temperature (20–25 °C). Currents were measured in the whole-cell patch clamp configuration using Pulse version 8.8 acquisition and stimulation software and an EPC10 amplifier (HEKA Elektronik, Lambrecht, Germany). Patch pipettes were pulled from borosilicate glass (KIMAX, Kimble Kontes, Mexico) and had resistances of 1.3–2.2 megohms when filled with intracellular solution (130 mM KCl, 1 mM $MgCl_2$, 5 mM EGTA, and 10 mM HEPES, pH 7.2). Cells were continuously superfused with extracellular solution containing 140 mM NaCl, 4 mM KCl, 1 mM $MgCl_2$, 2 mM $CaCl_2$, 10 mM glucose, and 10 mM HEPES, pH 7.35. Series resistance was compensated by 70%. A P/4 protocol was used for current density, activation, and long pulse protocols. Pulse protocols are described in the figure legends and text. Data were analyzed with Pulse/PulseFit (HEKA Elektronik, Lambrecht, Germany) and IGOR PRO (WaveMetric, Lake Oswego). Activation and inactivation curves were fitted with the Boltzmann function $P_o/P_{o,\,max} = \text{offset} + 1/(1 + \exp((V_m - V_{½})/a_h)$. A single exponential function, $y = \text{offset} + A_{exp}(-x/\tau)$ was used to calculate the activation time constants (τ) and to fit the cumulative frequency data. A double exponential function, $y = \text{offset} + A_{1,\,exp}(-x/\tau_1) + A_{2,\,exp}(-x/\tau_2)$, was used to fit closed-state inactivation and the recovery from inactivation data.

Yeast Two-hybrid Assay—The NH_2 termini of hKv2.1 (amino acids 3–186), hKv8.2 (amino acids 3–255), mKv8.2 (amino acids 3–263), hKv8.2-L126Q (amino acids 3–255), and mKv8.2-W196C (amino acids 3–263) were cloned into pLexN and pVP16. Yeast transformations and analyses were performed as described previously (14).

Cell Surface Biotinylation Assays—COS7L cells were transfected at 80–90% confluency with 4 μg of DNA using a Lipofectamine 2000 (Invitrogen) to DNA ratio of 2.5:1. For the study of homomeric Kv2.1 channels, 2 μg of Kv2.1-pcDNA3 or mutant Kv2.1-pcDNA3 was transfected, and for analysis of the surface expression of heteromeric Kv2.1/Kv8.2 channels, 2 μg of each channel subunit was transfected. 22 h post-transfection, cells were washed twice in ice-cold PBS(+) (PBS with 1 mM $CaCl_2$ and 0.5 mM $MgCl_2$) and then incubated with 0.5 mg/ml *N*-hydroxysulfosuccinimide-LC-biotin (Pierce) for 20 min at 4 °C. Cells were blocked in 1 mg/ml BSA in PBS(+), washed twice in blocking solution, and lysed in 100 μl of RIPA buffer (50 mM Tris, pH 7.5, 150 mM NaCl, 2 mM EGTA, 1 mM EDTA, 1% Nonidet P-40, 0.5% deoxycholate, 0.1% SDS, 1 mM PMSF, 1 μM leupeptin, 1 μM pepstatin) under constant rotation (1 h at 4 °C). Cell debris was removed by centrifugation (11,750 × *g*, 10 min, 4 °C), and 30 μl of neutravidin beads (50% slurry, Pierce) were added to the supernatant and incubated under rotation (2 h, 4 °C). Beads were washed twice in high salt RIPA (RIPA with 500 mM NaCl) followed by a final wash in standard RIPA. SDS sample buffer was added, and the proteins were eluted by heat denaturing (10 min, 95 °C), separated on 7.5% SDS-polyacrylamide gels, and transferred to nitrocellulose membranes. Kv2.1 was detected using the K89/34 antibody (1:1000) and a second-

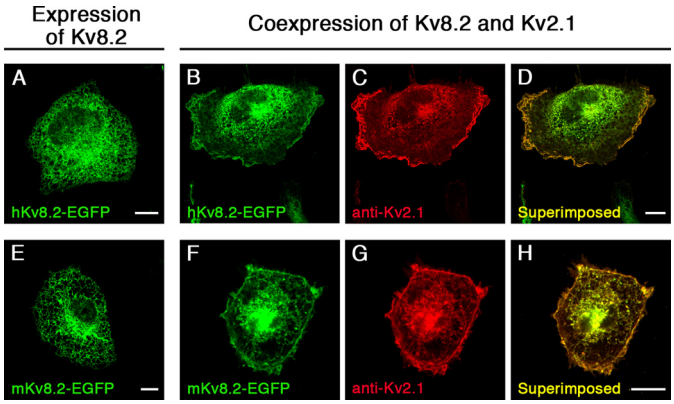

FIGURE 1. **Expression of Kv8.2 subunits in COS7L cells.** Kv8.2 α-subunits were expressed alone or together with the Kv2.1 α-subunit in COS7L cells. Confocal pictures show the following: *A,* expression of hKv8.2-EGFP; *B* and *C,* coexpression of hKv8.2-EGFP with hKv2.1; *D,* superimposition of *B* and *C*; *E,* expression of mKv8.2-EGFP; *F* and *G,* coexpression of mKv8.2-EGFP with mKv2.1; *H,* superimposition of *F* and *G*. Kv8.2 and Kv2.1 subunits were coexpressed in a 1:3 ratio. *Green fluorescence* indicates Kv8.2-EGFP subunits; *red fluorescence* indicates Kv2.1 subunits. *Scale bars,* 10 μm.

ary anti-mouse HRP-conjugated antibody (1:4000) (Bio-Rad). Protein bands were imaged using an ImageQuant LAS 4000 biomolecular imager (GE Healthcare) and analyzed in ImageJ (35). Mean gray values for surface Kv2.1 protein bands were presented as a percentage of whole-cell Kv2.1 (input) levels.

Statistical Analysis—Data were logarithmically transformed when not normally distributed or showed heteroscedasticity. Statistical analysis was performed using the Student's *t* test or one-way ANOVA followed by the Dunnett's or Bonferroni's multicomparison test. Data are presented as mean ± S.E. $p < 0.05$ was considered statistically significant. $p < 0.05$ and $p < 0.01$ are indicated in figures by * or **, respectively, and the number of experiments (n) is indicated above each bar.

RESULTS

Coexpression of Kv8.2 and Kv2.1 Subunits—The observation that α-subunits of the Kv5, Kv6, Kv8, and Kv9 subfamilies only form functional heteromeric channels with members of the Kv2 subfamily in heterologous expression systems led to their denomination as modulatory α-subunits. We examined the localization of mKv8.2 and hKv8.2 α-subunits, both tagged with EGFP at the COOH terminus, in COS7L cells. An intracellular localization with no apparent membrane expression was observed when either mKv8.2 or hKv8.2 was expressed (Fig. 1, *A* and *E*). Not surprisingly, the expression of hKv2.1 (see Fig. 6*A*) and mKv2.1 (data not shown) resulted instead in a clear signal at the plasma membrane. The coexpression of Kv8.2 with Kv2.1 also led to a clear signal at the plasma membrane, as shown by EGFP fluorescence for Kv8.2 (Fig. 1, *B* and *F*), antibody staining for Kv2.1 (Fig. 1, *C* and *G*), and the overlay of signals (Fig. 1, *D* and *H*). The most straightforward explanation for this observation was that as a consequence of the interaction between Kv2.1 and Kv8.2, the intracellular retention of Kv8.2 was overcome, and this resulted in an efficient trafficking of these α-subunits to the plasma membrane.

Electrophysiological Properties of the hKv2.1/hKv8.2 Channel—It has been previously shown that the expression of hKv8.2 in Ltk$^-$ cells (12) and mKv8.2 in *Xenopus* oocytes (17) does not lead to the formation of functional channels at the plasma membrane. To test whether expression of hKv8.2 could elicit functional currents in HEK293, transfected cells were stimulated with a range of protocols, but the resulting currents did not differ from mock-transfected cells (data not shown). The absence of Kv8.2 current is in agreement with the intracellular retention of Kv8.2 subunits (Fig. 1). Currents mediated by functional heteromeric hKv2.1/hKv8.2 channels were observed on coexpression of hKv8.2 and hKv2.1 (Fig. 2, *A–K*). Families of current traces elicited by 200-ms voltage steps, from −80 to +80 mV with 10-mV increments (Fig. 2*A*), showed current amplitudes clearly above background but revealed also a 6-fold reduction in current density at a voltage of +30 mV for hKv2.1/hKv8.2 (0.32 ± 0.06 nA/pF, $n = 17$) compared with hKv2.1 alone (2.04 ± 0.24 nA/pF, $n = 20$) (Fig. 2*B*). The open probability ($P_o/P_{o,\,max}$) voltage curve of hKv2.1 and hKv2.1/hKv8.2 channels showed similar values for half-maximal activation but significantly different slopes (a_n) (Fig. 2*C* and Table 1). In addition, the time course of activation was slightly faster at more negative potentials for hKv2.1/hKv8.2 channels (Fig. 2*D* and Table 1).

The most noticeable difference between the hKv2.1/hKv8.2 and hKv2.1 channels arises from their inactivation properties. During the application of a prolonged 10-s voltage step to +30 mV, hKv2.1/hKv8.2 channels inactivated more slowly (τ_{inact}, 3.7 ± 0.3 s, $n = 8$) than hKv2.1 channels (τ_{inact}, 2.8 ± 0.2 s, $n = 7$) (Fig. 2*E* and Table 1). At the end of this depolarization, the hKv2.1/hKv8.2 channel had inactivated by 70%, significantly less than the 90% observed for the hKv2.1 channel (Fig. 2*E* and Table 1). The estimated half-maximal inactivation voltage ($V_{h,½}$) of both channels was not significantly different (Fig. 2*F* and Table 1). Instead, whereas hKv2.1 channels showed a complete inactivation, hKv2.1/hKv8.2 channels never completely inactivated (Fig. 2*F*) even after prolonged inactivating prepulses of up to 60 s (data not shown).

In addition to affecting inactivation from open states, several modulatory α-subunits influence the inactivation from intermediate closed states (11, 19). hKv2.1/hKv8.2 channels showed reduced inactivation from intermediate closed states in comparison with hKv2.1 homomeric channels (Fig. 2*G*). Furthermore, rat (r) Kv2.1/rKv5.1, rKv2.1/rKv6.1, and rKv2.1/rKv9.3 heteromeric channels exhibit an accelerated rate of recovery from inactivation (11, 19). To determine the influence of hKv8.2 α-subunits on the time course of recovery from inactivation, the ratios of the current amplitudes obtained from 200-ms pulses to +60 mV (P1 and P3), before and after the channels were inactivated and allowed to recover, are plotted in Fig. 2*H* against the time spent at the recovery potential (−80 mV). hKv2.1/hKv8.2 heteromeric channels recovered substantially faster than homomeric hKv2.1 channels (Fig. 2*H*). Time constants for recovery were estimated by fitting double exponential functions to the data. Both the fast and slow time constants of recovery for hKv2.1/hKv8.2 channels ($\tau_{1,\,rec}$, 0.2 ± 0.03 s; $\tau_{2,\,rec}$, 1.9 ± 0.3 s, $n = 6$) were five times smaller than those for hKv2.1 channels ($\tau_{1,\,rec}$, 1.0 ± 0.08 s; $\tau_{2,\,rec}$, 8.5 ± 1.9 s, $n = 6$, $p < 0.01$).

Repetitive depolarizations can lead to a successive decline in current amplitude. This cumulative inactivation has been

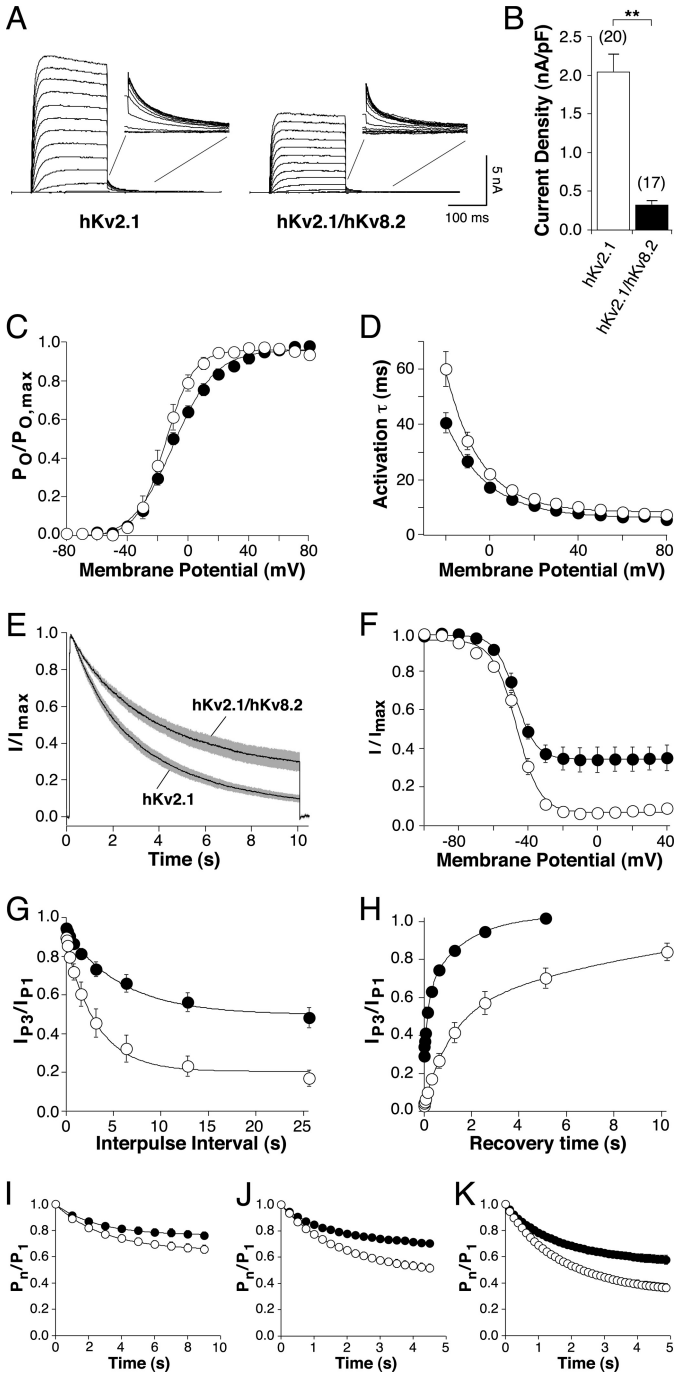

FIGURE 2. **Comparison of electrophysiological properties of hKv2.1 and hKv2.1/hKv8.2.** Throughout the figure, *open circle* is used for hKv2.1, and *filled circle* is used for hKv2.1/hKv8.2. *A,* hKv2.1 and hKv2.1/hKv8.2 currents recorded from HEK293 cells transfected with 90 ng of hKv2.1-pcDNA3 or cotransfected with hKv2.1-pcDNA3 and hKv8.2-pcDNA3 in a 1:1 ratio. Currents were elicited by 200-ms voltage steps from −80 to +80 mV (10-mV increments) followed by a step to −40 mV. *B, bar diagram* comparing the current densities obtained for homomeric hKv2.1 and heteromeric hKv2.1/hKv8.2 at +30 mV. *C,* voltage dependence of activation. Amplitudes of the tail currents obtained by the pulse protocol described in *A* were used. After normalization, the relative open probabilities derived from the initial currents were plotted against the voltage of the depolarizing step and fitted with a Boltzmann function ($n = 6–8$). *D,* voltage dependence of the time course of activation. τ_{act} was obtained from mono-exponential fits to current traces elicited by the 200-ms voltage steps described in *A* and plotted as a function of the test potential. *E,* inactivation from the open state. Currents elicited by a 10-s voltage step from −80 mV to +30 mV. *Solid lines* represent mean currents, and *gray shading* indicates the S.E. ($n = 7–8$). *F,* voltage dependence of the steady-state inactivation. Channels were inactivated for 20 s (hKv2.1) or 30 s (hKv2.1/hKv8.2) at prepulse potentials ranging from −100 to +40 mV, followed by a test pulse to +60 mV to activate residual noninactivated channels. The normalized amplitudes were plotted against the prepulse potentials and fitted with a Boltzmann function ($n = 7–9$). *G,* inactivation from intermediate closed states. After a 200-ms test pulse (P1) to +60 mV, channels were inactivated for an increasing time at −40 mV (P2), after which another 200-ms test pulse (P3) to +60 mV was applied. The proportion of current remaining (I_{P3}/I_{P1}) was plotted against the time spent at (P2) ($n = 8$). *H,* time dependence of recovery from inactivation. After a 200-ms test pulse to +60 mV (P1), a 20-s (hKv2.1) or 30-s (hKv2.1/hKv8.2) conditioning pulse to −10 mV was applied to obtain maximal inactivation. Recovery was measured by another 200-ms test pulse to +60 mV (P3) after increasing intervals at the recovery potential (−80 mV, P2). The proportion of recovered current (I_{P3}/I_{P1}) was plotted against the time spent at the recovery potential ($n = 6$). *I–K,* cumulative inactivation. Repeated depolarizing steps between −80 and +60 mV were applied at a frequency of 1 Hz (*I*), 4 Hz (*J*), or 8 Hz (*K*) with equal time spent at −80 and +60 mV. The normalized current amplitudes at each depolarization were plotted against time ($n = 6–13$).

TABLE 1

Biophysical properties of hKv2.1 and hKv2.1/hKv8.2 channels expressed in HEK293 cells

Kinetic parameters for activation ($V_{n,\frac{1}{2}}$, a_n) and inactivation ($V_{h,\frac{1}{2}}$, a_h) are given. Time constant of activation and inactivation (τ_{act} and τ_{inact}) is shown.

Biophysical property	hKv2.1	hKv2.1/hKv8.2
Activation		
Current density (nA/pF)	2.04 ± 0.24 ($n = 20$)	0.32 ± 0.06 ($n = 17$)[a]
$V_{n,\frac{1}{2}}$ (mV)	−14.6 ± 3.1 ($n = 8$)	−9.5 ± 1.6 ($n = 6$)
a_n (mV)	8.8 ± 0.9 ($n = 8$)	13.9 ± 1.0 ($n = 6$)[a]
τ_{act} at −20 mV (ms)	60.0 ± 6.2 ($n = 6$)	40.6 ± 3.7 ($n = 6$)[a]
10-s depolarization to +30 mV		
% inactivation	90.2 ± 2.1 ($n = 7$)	70.3 ± 5.1 ($n = 8$)[a]
$\tau_{inact\ (s)}$	2.8 ± 0.2 ($n = 7$)	3.7 ± 0.3 ($n = 8$)[a]
Steady-state inactivation		
$V_{h,\frac{1}{2}}$ (mV)	−46.8 ± 1.3 ($n = 9$)	−47.3 ± 1.5 ($n = 7$)
a_h (mV)	6.5 ± 0.3 ($n = 9$)	5.1 ± 0.5 ($n = 7$)[a]

[a] Significantly different properties ($p < 0.05$).

described for the rKv2.1 channel (36) and is a consequence of its preferential inactivation from intermediate closed states and slow recovery from inactivation. Because hKv2.1/hKv8.2 channels show a reduced inactivation from intermediate closed states and an accelerated recovery from inactivation, we hypothesized that these heteromeric channels may be less susceptible to cumulative inactivation. In particular, the faster time course of recovery from inactivation should enable a greater proportion of hKv2.1/hKv8.2 channels to recover during short hyperpolarizing steps between high frequency depolarizations. To test this hypothesis, repetitive depolarizations to +60 mV were applied at a frequency of 1 Hz (Fig. 2*I*), 4 Hz (Fig. 2*J*), or 8 Hz (Fig. 2*K*). As predicted, at all three frequencies tested, hKv2.1/hKv8.2 channels showed less cumulative inactivation than hKv2.1 channels.

Selection of Kv8.2 Mutations—With the exception of the S4 transmembrane region involved in voltage sensing, missense mutations are located throughout the channel protein in different cases of CDSRE (2, 26–33). In this study, we have selected five different mutations, three in the pore region that is responsible for ion conduction and two in the T1 domain that has been shown to be important in subunit assembly.

Analysis of Mutations Located in the Pore Domain of Kv8.2—Fig. 3 shows the location of the disease-causing mutations in hKv8.2 in CDSRE patients examined in this study. Three of these, W450G, G459D, and G461R, are located in the pore region of the hKv8.2 α-subunit. The missense mutations G459D and G461R affect the first and second glycine, respec-

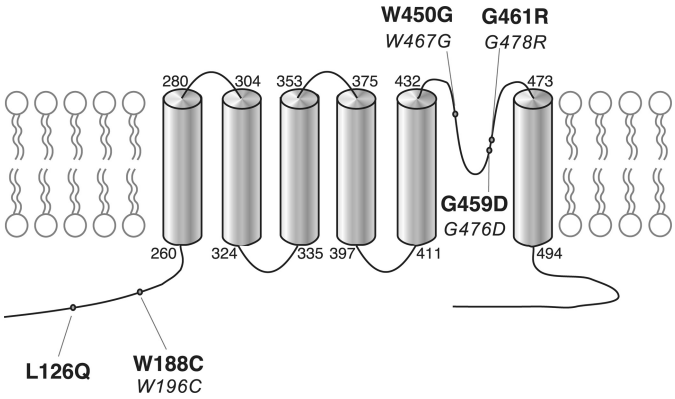

FIGURE 3. **Topological scheme of hKv8.2.** Shown is the location of the five missense disease mutations in *KCNV2* (2, 31) studied. The numbers in *boldface* correspond to the amino acid position in hKv8.2, and the numbers in *italic* correspond to the equivalent position in mKv8.2.

tively, of the Gly-Tyr-Gly motif, the characteristic potassium channel signature sequence. To understand the functional consequences of these mutations, the corresponding mutations (*W467G, G476D*, and *G478R*, Fig. 3) were introduced into mKv8.2, and their effect on subunit localization in COS7L cells was examined. Like mKv8.2, the expression of either mKv8.2-W467G-EGFP, mKv8.2-G476D-EGFP, or mKv8.2-G478R-EGFP resulted in an intracellular localization (Fig. 4, *A*, *E*, and *I*). When mKv8.2-W467G-EGFP was coexpressed with mKv2.1, the signal for both subunits was identified at the membrane (Fig. 4, *B–D*), suggesting that this mutant subunit is able to form heteromeric channels with mKv2.1, overcoming the retention and resulting in plasma membrane localization. A similar result was obtained with the coexpression of mKv8.2-G478R-EGFP subunits with mKv2.1 (Fig. 4, *J–L*). In contrast, the coexpression of mKv8.2-G476D-EGFP with mKv2.1 (Fig. 4, *F–H*) resulted in little or no fluorescence at the plasma membrane in the majority of cells, suggesting that both Kv8.2-G476D and Kv2.1 subunits were retained intracellularly.

To investigate the functional properties of channels containing mKv8.2-W467G, mKv8.2-G476D, or mKv8.2-G478R α-subunits, whole-cell recordings were performed on transiently transfected HEK293 cells. Like hKv8.2 (Fig. 2*B*), mKv8.2 forms functional heteromers with hKv2.1 resulting in reduced current densities (0.19 $\pm$ 0.05 nA/pF; Fig. 4*M*) and reduced inactivation from the open state (Fig. 4*N*). The hKv2.1-subunit was used for these coexpression experiments as the properties of hKv2.1 channels have been extensively characterized.

Cells expressing hKv2.1 and either mKv8.2-W467G or mKv8.2-G478R showed substantially lower current densities than those expressing the hKv2.1/mKv8.2 heteromer (Fig. 4*M*). This strongly suggests that although hKv2.1 and mKv8.2-W467G (Fig. 4, *B–D*) and hKv2.1 and mKv8.2-G478R (Fig. 4, *J–L*) were present at the plasma membrane and most likely incorporated into heteromeric channels, their ability to conduct was severely impaired. In contrast, expression of hKv2.1 and mKv8.2-G476D yielded current densities comparable with those of hKv2.1/mKv8.2 (Fig. 4*M*). The reported differences are supported by a one-way ANOVA ($F_{3,52} = 5.92$, $p = 0.0015$) followed by Dunnett's multiple comparison test (hKv2.1/mKv8.2 *versus* hKv2.1 and mKv8.2-W467G, $p < 0.01$; hKv2.1/

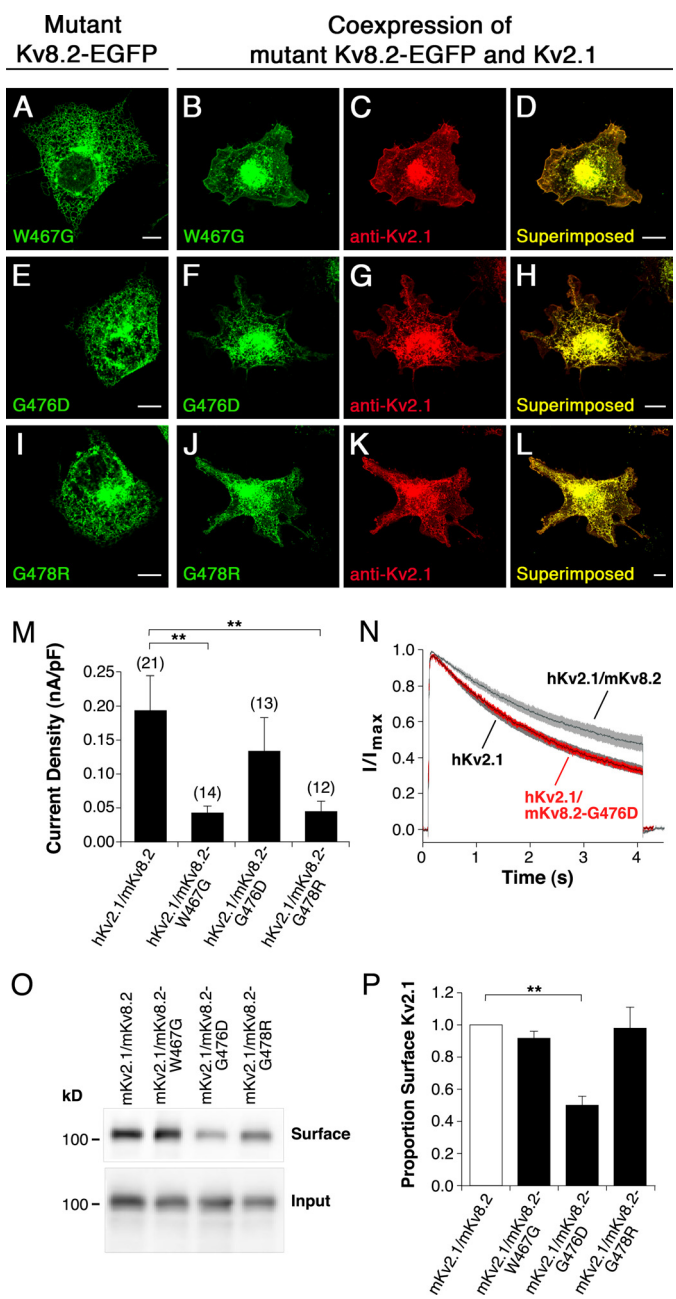

FIGURE 4. **Characterization of missense mutations located in the pore region of Kv8.2 (mKv8.2-W467G, mKv8.2-G476D, and mKv8.2-G478R).** Mutant α-subunits were expressed alone or together with mKv2.1 α-subunits in COS7L cells in a 1:3 ratio. Confocal pictures show the following. *A*, mKv8.2-W467G-EGFP; *B* and *C*, coexpression of mKv8.2-W467G-EGFP with mKv2.1; *D*, superimposition of *C* and *D*; *E*, mKv8.2-G476D-EGFP; *F* and *G*, coexpression of mKv8.2-G476D-EGFP with mKv2.1; *H*, superimposition of *F* and *G*; *I*, mKv8.2-G478R-EGFP; *J* and *K*, coexpression of mKv8.2-G478R-EGFP with mKv2.1; *L*, superimposition of *J* and *K*. *Green fluorescence* indicates mutant mKv8.2-EGFP subunits; *red fluorescence* indicates mKv2.1 subunits. *Scale bars*, 10 μm. *M*, current densities observed upon a voltage step to +30 mV in HEK293 cells expressing the indicated α-subunits: hKv2.1/mKv8.2 (0.19 $\pm$ 0.05 nA/pF, $n = 21$), hKv2.1/mKv8.2-W467G (0.043 $\pm$ 0.011 nA/pF, $n = 14$), hKv2.1/mKv8.2-G476D (0.13 $\pm$ 0.05 nA/pF, $n = 13$), and hKv2.1/mKv8.2-G478R (0.045 $\pm$ 0.015 nA/pF, $n = 12$). *N*, comparison of the inactivation from the open state of hKv2.1, hKv2.1/mKv8.2 (*gray*), and hKv2.1/mKv8.2-G476D (*red*). Currents were elicited by a 4-s depolarization to +30 mV. *Solid lines* represent the mean currents with shading indicating the S.E. *O*, surface expression of mKv2.1. The level of surface expression of mKv2.1 upon coexpression with mKv8.2, mKv8.2-W467G, mKv8.2-G476D, or mKv8.2-G478R in COS7L cells is shown. *P*, *bar diagram* showing the proportion of mKv2.1 in the plasma membrane for the different coexpressions indicated ($n = 3$). The expression level of the mKv2.1 heteromer was set to 1.

mKv8.2 *versus* hKv2.1 and mKv8.2-G478R, $p < 0.01$; hKv2.1/mKv8.2 *versus* hKv2.1 and mKv8.2-G476D, $p > 0.05$). Despite the similar current densities, the inactivation from the open state seen for the coexpression of hKv2.1 and mKv8.2-G476D did not resemble the behavior seen for hKv2.1/mKv8.2 but was instead identical to that of homomeric hKv2.1 channels. Indeed, the current traces for the inactivation of mKv8.2-G476D from the open state (shown in *red* in Fig. 4*N*) follow exactly those for the homomeric hKv2.1 channels (shown in *gray* in Fig. 4*N*). The simplest explanation for this observation is that coexpression of hKv2.1 and mKv8.2-G476D α-subunits results in a substantial retention of hKv2.1 α-subunits, with a limited number of Kv2.1 α-subunits escaping this retention and forming functional homomeric channels at the plasma membrane. This explains the large reduction in current density when compared with homomeric hKv2.1 channels (Fig. 2*B*) and, considered together with the kinetic behavior, suggests that the observed current is mediated solely by homomeric hKv2.1 channels.

If coexpression of Kv2.1 with Kv8.2 α-subunits carrying a pore mutation leads to the formation of heteromeric channels, Kv2.1 should be found at the plasma membrane. To quantify the amount of Kv2.1 α-subunits at the plasma membrane, we performed surface biotinylation experiments on COS7L cells coexpressing mKv2.1 with either mKv8.2, mKv8.2-W467G, mKv8.2-G476D, or mKv8.2-G478R. An effective biotinylation of mKv2.1 surface channels was achieved by transiently incubating transfected cells with the membrane-impermeable sulfo-*N*-hydroxysulfosuccinimide-LC biotin. After cell lysis, the biotin-labeled surface proteins were isolated with neutravidin resin, and mKv2.1 was quantified by Western blotting. The absence of α-tubulin from the biotinylated surface fraction demonstrated that no accidental permeabilization of the cells had occurred, and only membrane proteins had been labeled (data not shown). Comparable levels of mKv2.1 were found in the surface fraction upon coexpression with mKv8.2 (100%, $n = 3$), mKv8.2-W467G (91.6 ± 4.7%, $n = 3$), and mKv8.2-G478R (97.9 ± 0.1%, $n = 3$) (Fig. 4, *O* and *P*). However, the coexpression of mKv2.1 with mKv8.2-G476D led to a 50.1 ± 5.7% ($n = 3$) reduction in the amount of mKv2.1 in the membrane when compared with the coexpression of mKv2.1 and mKv8.2 (Fig. 4, *O* and *P*). The reported changes in the level of surface expression are supported by a one-way ANOVA ($F_{3,8} = 9.74$, $p = 0.005$) followed by Dunnett's multiple comparison test (mKv2.1/mKv8.2 *versus* mKv2.1 and mKv8.2-W467G, $p > 0.05$; mKv2.1/mKv8.2 *versus* hKv2.1 and mKv8.2-G478R, $p > 0.05$; hKv2.1/mKv8.2 *versus* hKv2.1 and mKv8.2-G476D, $p < 0.01$).

Mutations at the Intracellular Amino Terminus of Kv8.2—Two-thirds of the mutations identified in patients with CDSRE are located in the intracellular amino-terminal region of hKv8.2. Ten of these mutations result in the generation of a stop codon that would terminate translation before the first transmembrane spanning segment (S1) is reached. However, two of the initially identified missense mutations (2), L126Q and W188C, lie within the T1 domain (37). Because this domain is important for the assembly with the α-subunits of the Kv2 family, we examined how these mutations affect the properties of Kv2.1/Kv8.2 heteromeric channels. In particular, we asked whether these mutated α-subunits were still able to interact efficiently with Kv2.1 subunits, and if so, how this interaction affected their electrophysiological behavior. The W188C mutation was introduced at the corresponding position (W196C) in the mKv8.2 α-subunit, whereas L126Q was introduced into the hKv8.2 α-subunit.

As seen for Kv8.2 α-subunits (Figs. 1 and 4), the expression of both hKv8.2-L126Q-EGFP and mKv8.2-W196C-EGFP gave rise to an intracellular localization (Fig. 5, *A* and *E*). When hKv8.2-L126Q-EGFP was coexpressed with hKv2.1, only the red fluorescence corresponding to hKv2.1 α-subunits was observed at the plasma membrane (Fig. 5, *C* and *D*), whereas the hKv8.2-L126Q-EGFP remained intracellular (Fig. 5*B*), and the same distribution pattern was also seen for the coexpression of mKv8.2-W196C-EGFP and mKv2.1 (Fig. 5, *F–H*). The absence of a signal for hKv8.2-L126Q-EGFP and mKv8.2-W196C-EGFP in the plasma membrane suggests a lack of interaction between the mutant Kv8.2 and Kv2.1 α-subunits.

This hypothesis was further supported by the current densities observed in HEK293 cells transiently cotransfected with hKv2.1 and either hKv8.2-L126Q or mKv8.2-W196C (Fig. 5*I*). The comparable expression levels indicated by the current densities (Fig. 5*I*, one-way ANOVA, $F_{2,37} = 0.44$, $p = 0.65$) strongly suggest the exclusive formation of homomeric hKv2.1 channels. In addition, both coexpressions displayed half-maximal open probabilities ($P_{o,½}$) comparable with that of hKv2.1 channels (one-way ANOVA, $F_{3,22} = 2.31$, $p = 0.1$; Fig. 5*J*). A significant difference was seen in the slopes of the Boltzmann functions for hKv2.1 (8.8 ± 0.9 mV, $n = 8$), hKv2.1/hKv8.2 (13.9 ± 1.1, $n = 6$), and the coexpressions of hKv2.1 with hKv8.2-L126Q (9.1 ± 0.5 mV, $n = 6$) or mKv8.2-W196C (9.4 ± 0.7 mV, $n = 6$) (one-way ANOVA, $F_{3,22} = 8.29$, $p = 0.0007$). In fact, the Bonferroni's multiple comparison test showed that the slopes of the coexpressions of Kv2.1 with the amino-terminal mutated Kv8.2 channels were not different from those of homomeric hKv2.1 channels ($p > 0.05$), but they differed significantly from those of hKv2.1/hKv8.2 heteromeric channels ($p < 0.01$), supporting the idea that only homomeric Kv2.1 channels are formed in the presence of the amino-terminal mutated Kv8.2 subunits.

The currents observed at the end of a 10-s depolarizing pulse to +30 mV from cells coexpressing hKv2.1 and either hKv8.2-L126Q or mKv8.2-W196C showed inactivation properties similar to those of hKv2.1 channels. Cells coexpressing hKv2.1 and hKv8.2-L126Q α-subunits displayed a reduction of 87.1 ± 1.7% ($n = 14$), and cells coexpressing hKv2.1 and mKv8.2-W196C showed a reduction of 92.3 ± 2.1% ($n = 7$). This degree of inactivation is not significantly different from that displayed by hKv2.1 (90.2 ± 2.1%, $n = 7$) (one-way ANOVA, $F_{2,25} = 2.26$, $p = 0.13$, Fig. 5*K*). The voltage dependence of steady-state inactivation for the coexpression of hKv2.1 with either of the two amino-terminal mutated Kv8.2 α-subunits was also similar to that of hKv2.1 homomeric channels (Fig. 5*L*). Surprisingly, a small shift to hyperpolarized potentials was observed for $V_{h,½}$ of both coexpressions, hKv2.1 with hKv8.2-L126Q (−53.5 ± 1.7 mV) and hKv2.1 with mKv8.2-W196C (−50.7 ± 2.0 mV) compared with hKv2.1 (−46.8 ± 1.3 mV) (one-way ANOVA $F_{2,20} =$

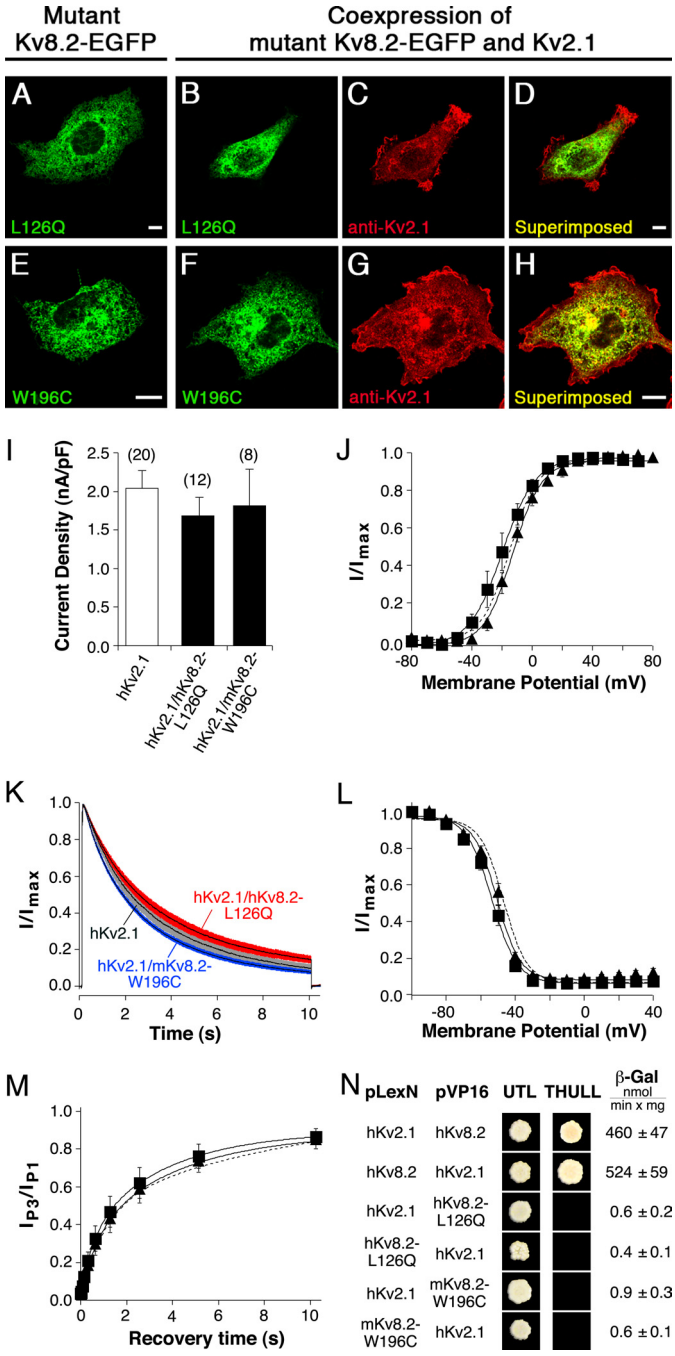

FIGURE 5. **Characterization of missense mutations located in the NH_2 terminus of Kv8.2 (hKv8.2-L126Q and mKv8.2-W196C).** Mutant α-subunits were expressed alone or together with the Kv2.1 α-subunit in COS7L cells in a 1:3 ratio. Confocal pictures show the following. *A,* hKv8.2-L126Q-EGFP; *B* and *C,* coexpression of hKv8.2-L126Q-EGFP with hKv2.1; *D,* superimposition of *B* and *C*; *E,* mKv8.2-W196C-EGFP; *F* and *G,* coexpression of mKv8.2-W196C-EGFP with mKv2.1; *H,* superimposition of *F* and *G*. *Green fluorescence* indicates mutant Kv8.2-EGFP subunits; *red fluorescence* indicates Kv2.1 α-subunits. *Scale bars,* 10 μm. *I, bar diagram* summarizing the current densities observed in HEK 293 cells expressing the indicated α-subunits: hKv2.1 (2.04 $\pm$ 0.24 nA/pF, $n = 20$), hKv2.1/hKv8.2-L126Q (1.68 $\pm$ 0.24 nA/pF, $n = 12$), and hKv2.1/mKv8.2-W196C (1.81 $\pm$ 0.48 nA/pF, $n = 8$). *J,* voltage dependence of activation on coexpression of hKv2.1 with hKv8.2-L126Q (■) and hKv2.1 with mKv8.2-W196C (▲). The *dashed line* corresponds to the voltage dependence of activation observed for hKv2.1 (Fig. 2*C*). *K,* comparison of the inactivation from the open state on coexpression of hKv2.1 with hKv8.2-L126Q (*red*), hKv2.1 with mKv8.2-W196C (*blue*), or expression of hKv2.1 (*gray*). Currents were elicited by a 10-s voltage step to +30 mV. *Solid lines* represent mean currents with shading indicating the S.E. *L,* voltage dependence of the steady-state inactivation. For the coexpression of hKv2.1 with hKv8.2-L126Q (■) and for hKv2.1 with hKv8.2-W196C (▲), channels were inactivated for 20 s at prepulse potentials ranging from −100 mV to +40 mV, followed by a test pulse to +60 mV to activate residual noninactivated channels. The Boltzmann curve obtained for hKv2.1 (Fig. 2*F*) is shown for comparison (*dashed line*). *M,* time dependence of the recovery from inactivation for the coexpressions of hKv2.1 with hKv8.2-L126Q (■) and hKv2.1 with mKv8.2-W196C (▲). The pulse protocol was identical to that described in Fig. 2*H* for the homomeric hKv2.1 channel. The exponential fit obtained for the recovery of hKv2.1 (from Fig. 2*H*) is shown for comparison (*dashed line*). *N,* yeast two-hybrid assay probing the homo- and heteromeric interactions mediated by the indicated NH_2 termini. Growth observed after pairwise transformation of yeast two-hybrid constructs pLexN-KvX.Y and pVP16-KvX.Y (indicated on the *left*) on UTL^- medium indicates successful transformation and growth on $THULL^-$ medium indicates interaction of fusion proteins. The *last column* shows the mean values obtained for the semi-quantitative test of interaction using the β-gal reporter gene.

4.84, $p = 0.02$). However, the slopes (a_h) of the coexpressions were similar to that of the hKv2.1 homomer (one-way ANOVA, $F_{2,20} = 0.1$, $p = 0.91$). Additionally, a more complete inactivation at depolarized potentials was observed (Fig. 5*L*), again resembling the behavior of the Kv2.1 homomer rather than the Kv2.1/Kv8.2 heteromer (Fig. 2*F*). Likewise, the recovery from inactivation showed the same slow time course as that of hKv2.1 homomers (Fig. 5*M*). Taken together, the similar electrophysiological characteristics of hKv2.1 homomers and the coexpressed amino-terminal mutated Kv8.2 α-subunits with Kv2.1 suggest that hKv8.2-L126Q and mKv8.2-W196C α-subunits do not assemble into heteromeric channels with hKv2.1.

The yeast two-hybrid system has been used by us and others to demonstrate interactions between T1 domains of modulatory and Kv2.1 α-subunits (11–14, 38). It was therefore employed to directly test the potential influence of the T1 domain mutations on the interaction between Kv2.1 and Kv8.2 α-subunits. The NH_2 termini, including the T1 domains of hKv2.1, hKv8.2, hKv8.2-L126Q, and mKv8.2-W196C, were cloned into pLexN to generate fusion proteins with the DNA binding domain LexA and also into pVP16 to produce fusion proteins with the VP16 DNA activation domain. The various constructs were then transformed pairwise into L40 yeast to identify interacting partners. Additionally the semiquantitative β-galactosidase assay was performed. As anticipated, the NH_2 terminus of hKv8.2 and mKv8.2 interacted with that of hKv2.1 in both configurations tested (Fig. 5*N*, *1st* and *2nd row*, only results for hKv8.2 are shown). However, neither the NH_2 terminus of hKv8.2-L126Q nor that of mKv8.2-W196C interacted with hKv2.1 in any configurations tested. As expected, no interaction of mKv8.2 with hKv8.2-L126Q or mKv8.2-W196C was observed (data not shown). These experiments confirm that both mutations, hKv8.2-L126Q and mKv8.2-W196C, disrupt the NH_2 terminus-directed heteromeric association between Kv8.2 and Kv2.1 α-subunits.

Amino-terminal Mutations That Disrupt Homomeric Interaction of Kv2.1 α-Subunits—An alignment of the cytoplasmic NH_2 termini of hKv8.2 and hKv2.1 showed that amino acids Leu-126 and Trp-188 are conserved in hKv2.1. Because mutation of these two residues in Kv8.2 disrupts the heteromeric interaction with Kv2.1, we examined whether the corresponding mutations in hKv2.1, hKv2.1-L60Q, and hKv2.1-W122C affect the homomeric interaction between Kv2.1 α-subunits. Confocal microscopy showed a clear signal at the plasma mem-

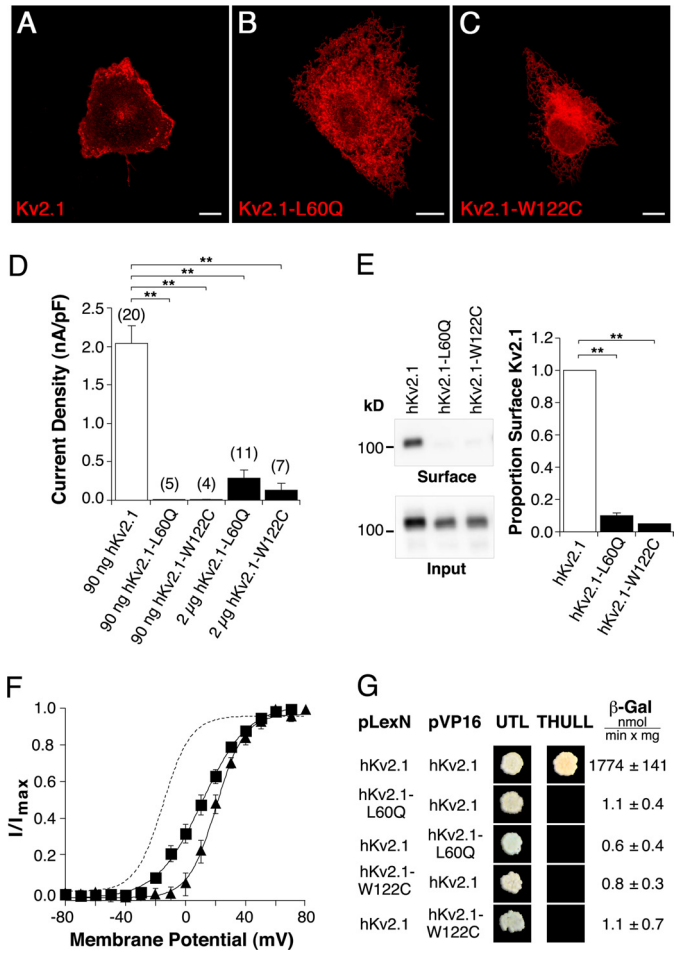

FIGURE 6. **Functional consequences of amino-terminal missense mutations on hKv2.1 channel characteristics.** hKv2.1-L60Q corresponds to hKv8.2-L126Q, and hKv2.1-W122C corresponds to hKv8.2-W188C. Confocal pictures show the following expression: *A,* hKv2.1; *B,* hKv2.1-L60Q; and *C,* hKv2.1-W122C in COS7L cells. *Red fluorescence* indicates hKv2.1 α-subunits. *Scale bars*, 10 μm. *D,* bar diagram summarizing the current densities observed in HEK293 cells expressing the indicated α-subunits. *E,* immunoblot revealing the surface expression of hKv2.1, hKv2.1-L60Q, and hKv2.1-W122C in COS7L cells. *Bar diagram* showing the proportion of hKv2.1-L60Q ($n = 3$) and hKv2.1-W122C ($n = 3$) that reach the plasma membrane with respect to hKv2.1. *F,* voltage dependence of activation of hKv2.1-L60Q (■) and hKv2.1-W122C (▲) channels. The *dashed line* corresponds to the voltage dependence of activation observed for hKv2.1 (Fig. 2*C*). *G,* results of the yeast two-hybrid assay. Growth observed after pairwise transformation of yeast two-hybrid constructs pLexN-KvX.Y and pVP16-KvX.Y (indicated on the *left*) on UTL^- medium indicates successful transformation, and growth on $THULL^-$ medium indicates interaction of the fusion proteins. The *last column* shows the mean values obtained for the semiquantitative test of interaction using the β-gal reporter gene.

brane of COS7L cells expressing hKv2.1 (Fig. 6*A*). In contrast, hKv2.1-L60Q (Fig. 6*B*) and hKv2.1-W122C (Fig. 6*C*) showed a mainly intracellular localization, suggesting a problem with the assembly or trafficking of these α-subunits. Next, we transfected HEK293 cells with hKv2.1, hKv2.1-L60Q, or hKv2.1-W122C and compared the overall current densities resulting from expression of these subunits (Fig. 6*D*). When the standard amount of 90 ng of DNA was used for transfection, no currents were observed for hKv2.1-L60Q (10.7 ± 4.3 pA/pF, $n = 5$) or hKv2.1-W122C (12.9 ± 5.6 pA/pF, $n = 4$). However, when the amount of hKv2.1-L60Q and hKv2.1-W122C DNA was increased to 2 μg, K^+ currents were observed, but current densities were still considerably smaller than for hKv2.1 (hKv2.1-L60Q, 0.28 ± 0.11 nA/pF, $n = 11$; hKv2.1-W122C, 0.13 ± 0.10 nA/pF, $n = 7$), which is consistent with a reduced ability of the mutated α-subunits to form functional channels at the plasma membrane. This observation was further supported by the cell surface biotinylation assay, to quantitate the amount of mutant α-subunit incorporated into the plasma membrane. The plasma membrane level of hKv2.1-L60Q was reduced to 10.0 ± 2.1% ($n = 3$) and that of hKv2.1-W122C to 4.9 ± 0.2% ($n = 3$) compared with hKv2.1 (Fig. 6*E*).

Expression of Kv2.1 α-subunits truncated at the NH_2 terminus also gave rise to low current densities in *Xenopus* oocytes. Furthermore, the voltage dependence of activation of these channels was shifted to more depolarized potentials (39). Similarly, hKv2.1-L60Q and hKv2.1-W122C channels displayed a shift in their voltage dependence of activation (Fig. 6*F*), suggesting that by preventing T1 domain interaction, the mutations introduce a change that is comparable with the lack of the T1 domain. We therefore tested the interaction capabilities of the mutated NH_2 termini directly using the yeast two-hybrid assay. Although the NH_2 termini of hKv2.1 interact with each other (Fig. 6*G*), the absence of growth on $THULL^-$ media for all other combinations tested demonstrates the inability of hKv2.1-L60Q and hKv2.1-W122C to interact with hKv2.1 (Fig. 6*G*) or with themselves (data not shown).

DISCUSSION

Modulatory subunits, also known as electrically silent subunits, form a large group of K^+ channel proteins that structurally resemble voltage-gated α-subunits. Their inability to form functional homomeric channels in heterologous expression systems hampered their functional analysis until suitable partners were identified, allowing an electrophysiological characterization. So far, only coexpression with Kv2 α-subunits, predominantly Kv2.1, has enabled functional expression and detailed biophysical insights. Little is known about the physiological function of channels formed with modulatory subunits (25). Recently, however, mutations in *KCNV2*, the gene that encodes the Kv8.2 α-subunit, have been identified in patients with the distinctive retinal disorder CDSRE, implying that the functional changes induced by these mutations led to the disease (2, 26–33). Here, we have characterized the effects of mutations in the pore region and T1 domain of the Kv8.2 α-subunit on the molecular physiology of Kv2.1/Kv8.2 heteromeric channels. Each of the five Kv8.2 mutations results in a loss of function of the Kv8.2 subunit leading to the functional abolition of the Kv2.1/Kv8.2 heteromer. For the T1 domain Kv8.2 mutants, this is accompanied by a related increase in Kv2.1 homomeric channels. Furthermore, our observations suggest physiologically distinct roles for Kv2.1/Kv8.2 heteromeric channels and homomeric Kv2.1 channels.

The expression of hKv2.1 and hKv2.1/hKv8.2 channels in HEK293 cells showed hyperpolarized shifts of the activation threshold and the voltages of half-maximal activation and inactivation in comparison with other studies (12, 17). The Kv2.1 channel is dynamically regulated by phosphorylation. Sixteen phosphorylation sites have been identified, which modulate its voltage dependence (40). Differences in the voltage dependence

of Kv2.1 in COS1 cells compared with HEK293 cells have been attributed to a different degree of phosphorylation of the channels (41). In addition, sphingomyelin interacts with the gating machinery of Kv2.1 thereby influencing its voltage dependence (42, 43). Different degrees of phosphorylation and different availabilities of sphingomyelin in distinct cell types might shift the voltage dependence of Kv2.1-containing channels to varying degrees. This may explain the differences in the voltage-dependence of the Kv2.1/Kv8.2 channels observed in different heterologous expression systems.

Compared with homomeric Kv2.1 channels, heteromeric hKv2.1/hKv8.2 channels show a reduced inactivation from the open state (this study and see Ref. 17), less inactivation from intermediate closed states, and as with Kv2.1/Kv5.1, Kv2.1/Kv6.1, and Kv2.1/Kv9.3 channels (11, 14), a faster recovery from inactivation. In comparison with Kv2.1, the reduced inactivation from the open state would allow heteromeric Kv2.1/Kv8.2 channels to remain open for longer in response to sustained depolarizations. The reduced inactivation from intermediate closed states would enable Kv2.1/Kv8.2 channels to activate in response to depolarizations from membrane potentials close to the activation threshold for these channels. Furthermore, depolarizations close to the activation threshold would result in a quicker response because Kv2.1/Kv8.2 channels display accelerated activation at negative potentials. The faster time course of recovery from inactivation, coupled with the reduced inactivation from open and closed states, would result in fewer Kv2.1/Kv8.2 channels in the inactivated state, in comparison with Kv2.1 homomeric channels. Altogether these variations in channel kinetics would enable cells expressing Kv8.2 or indeed other modulatory subunits to fine-tune their response to alterations in the membrane potential and thereby introduce functional diversity to the role of Kv2.1-containing channels.

The formation of Kv2.1/Kv8.2 heteromers is accompanied by a reduction in current density compared with Kv2.1 homomers, a consequence of Kv2.1 being retained by Kv8.2 α-subunits. Our analysis of the effect of the coexpression of Kv2.1 with three Kv8.2 disease mutations, W450G, G459D, and G478R (2, 31), all located in the pore region, showed a lack of any current resembling that produced by heteromeric Kv2.1/Kv8.2 channels. Intracellular retention in a fine reticular network, most likely the endoplasmic reticulum, has been reported for hKv8.2 in Ltk^- cells (12) and was shown in this study for hKv8.2 and mKv8.2 in HEK293 cells. Similarly, intracellular retention was observed for the three Kv8.2 pore mutations analyzed. The molecular mechanism of retention, observed also for other modulatory α-subunits, remains uncertain however (25).

When coexpressed with hKv2.1, mutant mKv8.2-W467G and mKv8.2-G478R subunits were trafficked to the plasma membrane, but a substantially lower residual current density was present compared with Kv2.1/Kv8.2 heteromers. The presence of nonconducting heteromeric Kv2.1/Kv8.2 channels in the plasma membrane of HEK293 cells is supported by surface biotinylation assays that show equal amounts of Kv2.1 present in the membrane fraction regardless of whether Kv2.1 is coexpressed with mKv8.2, mKv8.2-W467G, or mKv8.2-G478R. Disease mutations affecting the pore regions of Kv7.2 and Kv7.3, which form heteromers (44), and Kv11.1 (45) have also been shown to result in nonconducting surface-expressed channels.

In contrast, coexpression of Kv2.1 with mKv8.2-G476D, performed under conditions designed to avoid competition for protein synthesis or trafficking machinery, showed considerably fewer Kv2.1 subunits in the plasma membrane and a substantially reduced current density with the residual current resembling that of homomeric Kv2.1 channels. Kv8.2-G476D might therefore affect the assembly or trafficking of heteromeric channels and, under our heterologous conditions, may allow the escape of a limited number of Kv2.1 homomeric channels to the plasma membrane.

Recently, histidine 105, located in the T1 domain of Kv2.1, has been shown to selectively disrupt the heteromerization with the modulatory subunits Kv6.3 and Kv6.4 (38). Additionally, two negatively charged amino acids present in Kv2.1 and all modulatory α-subunits have been shown to be essential for the efficient assembly of homomeric Kv2.1 and heteromeric Kv2.1/Kv6.4 channels (46). Two disease mutations were examined, L126Q and W188C, that are located in the T1 domain of Kv8.2 at sites that are conserved in all modulatory subunits and in Kv2.1. Both mutants showed an intracellular distribution pattern indistinguishable from the one observed for Kv8.2 α-subunits, demonstrating that they do not result in general misfolding or fast degradation of the protein. However, the currents observed on coexpression of mutant Kv8.2 and Kv2.1 showed the same voltage dependence, kinetics, and density as homomeric Kv2.1 channels, indicating that these mutations efficiently prevent the interaction with Kv2.1 α-subunits. The inability of the mutated T1 domains of Kv8.2 to interact with the T1 domains of Kv2.1 was confirmed by yeast two-hybrid assay.

When L126Q and W188C were introduced at the corresponding positions in Kv2.1, they showed an intracellular retention resembling that of Kv8.2 α-subunits, and further experimentation supported the hypothesis of intracellular retention rather than an increase in protein degradation as a cause for reduced current densities. The absence of mutated α-subunits in the plasma membrane and the reduced currents can be viewed therefore as indications that the mutations prevent an efficient interaction of the Kv2.1 T1 domains. Kv channels assemble also in the absence of a functional T1 domain, albeit less efficiently (5, 39, 47, 48); this would account for the small amount of current and Kv2.1 α-subunit detected in the plasma membrane after transfection with large amounts of mutant Kv2.1. Finally, the yeast two-hybrid assay showed an absence of any interaction between mutated and nonmutated Kv2.1 NH_2 termini. The shift in the voltage dependence of activation of mutated Kv2.1 channels is not surprising, because changes to both the NH_2 and COOH termini influence the gating of Kv2.1 (39).

Our studies of the several mutations located in the pore and T1 domain of Kv8.2 allow us to postulate the existence of two distinct mechanisms involved in the disease pathology. Pore mutations lead simply to the formation of nonconducting heteromeric Kv2.1/Kv8.2 channels, whereas T1 domain mutations lead to the formation of homomeric Kv2.1 channels only. The mutations permitting the formation of homomeric Kv2.1 chan-

nels behave similarly to mutations that result in the absence of Kv8.2 α-subunits, whether by gene deletion, frameshift mutation, or premature termination (49). Interestingly, no clinical differences have been observed between patients harboring these different classes of mutations (30).

The presence of Kv8.2 mRNA in rod and cone photoreceptors (2, 17), together with the distinctive alteration in photoreceptor function in CDSRE, strongly suggest a role for Kv8.2 in retinal signal transduction, although its exact mechanism of action remains uncertain. Cone photoreceptors within the foveal region appear to be relatively more susceptible to damage by Kv8.2 mutations, whereas rod photoreceptors appear less affected (30). The latter observation is in agreement with the normal amplitude of the a-wave of the rod ERG in CDSRE patients. Therefore, it is likely that Kv8.2 is involved in shaping the signal response to light, because Kv8.2 mutations lead to severely impaired visual responses.

Absorption of photons in the outer segments of photoreceptors results in the closure of cyclic nucleotide gated (CNG) channels and membrane hyperpolarization from dark resting levels. Two currents are responsible for shaping this response, an inward current, I_h, which is activated by large hyperpolarizations, and a sustained outward current, I_{Kx}, which is responsible for shaping responses to dim light (50). In addition, in the dark, I_{Kx} opposes the inward current through CNG channels and so is responsible for setting the dark resting membrane potential. I_{Kx} currents have been identified in the photoreceptors of several mammalian species (51–54). In view of similar kinetic and pharmacological properties, it has been suggested that Kv2.1/Kv8.2 heteromers may contribute to the I_{Kx} current (17). Because of differences in channel kinetics and voltage dependences, Kv2.1/Kv8.2 heteromeric channels, but importantly not Kv2.1 homomeric channels, are able to maintain a sustained outward current in response to current injection, replicating the "dark current" of photoreceptors (17). Furthermore, cessation of this current injection, mimicking the onset of light, leads to a transient hyperpolarization that is required for the acceleration of the response (17). If this interpretation is correct and Kv2.1/Kv8.2 does underlie I_{Kx}, then the loss of functional Kv2.1/Kv8.2 heteromers, as demonstrated here, would result in membrane depolarization and a slowing of the light response. Membrane depolarization would in turn result in an increase in the threshold required to activate I_h and shape high intensity light responses. These predictions correlate well with the clinical findings. The characteristic ERG of CDSRE patients includes a severe reduction in the amplitude and a delay in the time course of responses to dim light, whereas responses to high intensity light are normal or even enhanced. A complicating issue is that the T1 domain Kv8.2 mutations result in a related increase in Kv2.1 homomers. However, because of the pronounced inactivation characteristics of the Kv2.1 channels, Kv2.1 homomers are unable to produce a sustained outward current (17) and so could not contribute to I_{Kx}. Therefore, the presence or absence of Kv2.1 subunits in the photoreceptors may be irrelevant because the Kv2.1 channels will remain in an inactivated state. This may provide an explanation for the lack of clinical differences between patients harboring the different classes of Kv8.2 mutations.

More in-depth analysis of native photoreceptor currents is required to confirm whether Kv2.1/Kv8.2 heteromers are the sole molecular correlates of I_{Kx}. Other channels, including Kv10.1 and Kv10.2, have also been proposed as candidates underlying the I_{Kx} current (55). Furthermore, the kinetic behavior of Kv2.1, and most likely also of Kv2.1/Kv8.2, is influenced by phosphorylation and membrane composition, making direct comparisons between native I_{Kx} and currents of recombinant channels rather difficult. Therefore, a specific Kv8.2 blocker or a genetic approach to suppress Kv8.2 is needed to reveal *in vivo* the currents generated by Kv2.1/Kv8.2 heteromers.

Mutations in genes encoding K^+ channels cause a number of diverse disease phenotypes, including long QT syndrome, epilepsy (56, 57), and snowflake vitreoretinal degeneration (58). Kv8.2 is the first modulatory Kv α-subunit to be linked to a human disease. Potassium channels are the obvious candidates for the development of treatments for potassium channelopathies. Moreover, for CDSRE, it would appear that structural damage within the retina is delayed, thereby providing a window of opportunity during which therapeutic intervention may prove successful (30). However, for this to be achieved, a more complete understanding of the role of Kv8.2 in phototransduction is required.

Acknowledgment—We thank Dr. P. Pedarzani for scientific discussions and critical reading of the manuscript.

REFERENCES

1. Gouras, P., Eggers, H. M., and MacKay, C. J. (1983) Cone dystrophy, nyctalopia, and supernormal rod responses. A new retinal degeneration. *Arch. Ophthalmol.* **101,** 718–724
2. Wu, H., Cowing, J. A., Michaelides, M., Wilkie, S. E., Jeffery, G., Jenkins, S. A., Mester, V., Bird, A. C., Robson, A. G., Holder, G. E., Moore, A. T., Hunt, D. M., and Webster, A. R. (2006) Mutations in the gene *KCNV2* encoding a voltage-gated potassium channel subunit cause cone dystrophy with supernormal rod electroretinogram in humans. *Am. J. Hum. Genet.* **79,** 574–579
3. Gutman, G. A., Chandy, K. G., Grissmer, S., Lazdunski, M., McKinnon, D., Pardo, L. A., Robertson, G. A., Rudy, B., Sanguinetti, M. C., Stühmer, W., and Wang, X. (2005) International Union of Pharmacology. LIII. Nomenclature and molecular relationships of voltage-gated potassium channels. *Pharmacol. Rev.* **57,** 473–508
4. Yellen, G. (2002) The voltage-gated potassium channels and their relatives. *Nature* **419,** 35–42
5. Li, M., Jan, Y. N., and Jan, L. Y. (1992) Specification of subunit assembly by the hydrophilic amino-terminal domain of the *Shaker* potassium channel. *Science* **257,** 1225–1230
6. Shen, N. V., and Pfaffinger, P. J. (1995) Molecular recognition and assembly sequences involved in the subfamily-specific assembly of voltage-gated K^+ channel subunit proteins. *Neuron* **14,** 625–633
7. Lee, T. E., Philipson, L. H., Kuznetsov, A., and Nelson, D. J. (1994) Structural determinant for assembly of mammalian K^+ channels. *Biophys. J.* **66,** 667–673
8. Christie, M. J., North, R. A., Osborne, P. B., Douglass, J., and Adelman, J. P. (1990) Heteropolymeric potassium channels expressed in *Xenopus* oocytes from cloned subunits. *Neuron* **4,** 405–411
9. Isacoff, E. Y., Jan, Y. N., and Jan, L. Y. (1990) Evidence for the formation of heteromultimeric potassium channels in *Xenopus* oocytes. *Nature* **345,** 530–534
10. Ruppersberg, J. P., Schröter, K. H., Sakmann, B., Stocker, M., Sewing, S., and Pongs, O. (1990) Heteromultimeric channels formed by rat brain potassium-channel proteins. *Nature* **345,** 535–537

11. Kramer, J. W., Post, M. A., Brown, A. M., and Kirsch, G. E. (1998) Modulation of potassium channel gating by coexpression of Kv2.1 with regulatory Kv5.1 or Kv6.1 α-subunits. *Am. J. Physiol.* **274,** C1501–C1510
12. Ottschytsch, N., Raes, A., Van Hoorick, D., and Snyders, D. J. (2002) Obligatory heterotetramerization of three previously uncharacterized Kv channel α-subunits identified in the human genome. *Proc. Natl. Acad. Sci. U.S.A.* **99,** 7986–7991
13. Post, M. A., Kirsch, G. E., and Brown, A. M. (1996) Kv2.1 and electrically silent Kv6.1 potassium channel subunits combine and express a novel current. *FEBS Lett.* **399,** 177–182
14. Stocker, M., Hellwig, M., and Kerschensteiner, D. (1999) Subunit assembly and domain analysis of electrically silent K^+ channel α-subunits of the rat Kv9 subfamily. *J. Neurochem.* **72,** 1725–1734
15. Castellano, A., Chiara, M. D., Mellström, B., Molina, A., Monje, F., Naranjo, J. R., and López-Barneo, J. (1997) Identification and functional characterization of a K^+ channel α-subunit with regulatory properties specific to brain. *J. Neurosci.* **17,** 4652–4661
16. Chiara, M. D., Monje, F., Castellano, A., and López-Barneo, J. (1999) A small domain in the N terminus of the regulatory α-subunit Kv2.3 modulates Kv2.1 potassium channel gating. *J. Neurosci.* **19,** 6865–6873
17. Czirják, G., Tóth, Z. E., and Enyedi, P. (2007) Characterization of the heteromeric potassium channel formed by Kv2.1 and the retinal subunit Kv8.2 in *Xenopus* oocytes. *J. Neurophysiol.* **98,** 1213–1222
18. Hugnot, J. P., Salinas, M., Lesage, F., Guillemare, E., de Weille, J., Heurteaux, C., Mattéi, M. G., and Lazdunski, M. (1996) Kv8.1, a new neuronal potassium channel subunit with specific inhibitory properties toward Shab and Shaw channels. *EMBO J.* **15,** 3322–3331
19. Kerschensteiner, D., and Stocker, M. (1999) Heteromeric assembly of Kv2.1 with Kv9.3. Effect on the state dependence of inactivation. *Biophys. J.* **77,** 248–257
20. Patel, A. J., Lazdunski, M., and Honoré, E. (1999) Kv2.1/Kv9.3, an ATP-dependent delayed-rectifier K^+ channel in pulmonary artery myocytes. *Ann. N.Y. Acad. Sci.* **868,** 438–441
21. Salinas, M., de Weille, J., Guillemare, E., Lazdunski, M., and Hugnot, J. P. (1997) Modes of regulation of shab K^+ channel activity by the Kv8.1 subunit. *J. Biol. Chem.* **272,** 8774–8780
22. Salinas, M., Duprat, F., Heurteaux, C., Hugnot, J. P., and Lazdunski, M. (1997) New modulatory α-subunits for mammalian shab K^+ channels. *J. Biol. Chem.* **272,** 24371–24379
23. Zhu, X. R., Netzer, R., Böhlke, K., Liu, Q., and Pongs, O. (1999) Structural and functional characterization of Kv6.2 a new γ-subunit of voltage-gated potassium channel. *Receptors Channels* **6,** 337–350
24. Kerschensteiner, D., Soto, F., and Stocker, M. (2005) Fluorescence measurements reveal stoichiometry of K^+ channels formed by modulatory and delayed rectifier α-subunits. *Proc. Natl. Acad. Sci. U.S.A.* **102,** 6160–6165
25. Bocksteins, E., and Snyders, D. J. (2012) Electrically silent Kv subunits: their molecular and functional characteristics. *Physiology* **27,** 73–84
26. Ben Salah, S., Kamei, S., Sénéchal, A., Lopez, S., Bazalgette, C., Bazalgette, C., Eliaou, C. M., Zanlonghi, X., and Hamel, C. P. (2008) Novel *KCNV2* mutations in cone dystrophy with supernormal rod electroretinogram. *Am. J. Ophthalmol.* **145,** 1099–1106
27. Khan, A. O., Alrashed, M., and Alkuraya, F. S. (2012) Cone dystrophy with supranormal rod response in children. *Br. J. Ophthalmol.* **96,** 422–426
28. Littink, K. W., Koenekoop, R. K., van den Born, L. I., Collin, R. W., Moruz, L., Veltman, J. A., Roosing, S., Zonneveld, M. N., Omar, A., Darvish, M., Lopez, I., Kroes, H. Y., van Genderen, M. M., Hoyng, C. B., Rohrschneider, K., van Schooneveld, M. J., Cremers, F. P., and den Hollander, A. I. (2010) Homozygosity mapping in patients with cone-rod dystrophy. Novel mutations and clinical characterizations. *Invest. Ophthalmol. Vis. Sci.* **51,** 5943–5951
29. Robson, A. G., Webster, A. R., Michaelides, M., Downes, S. M., Cowing, J. A., Hunt, D. M., Moore, A. T., and Holder, G. E. (2010) Cone dystrophy with supernormal rod electroretinogram. A comprehensive genotype/phenotype study including fundus autofluorescence and extensive electrophysiology. *Retina* **30,** 51–62
30. Sergouniotis, P. I., Holder, G. E., Robson, A. G., Michaelides, M., Webster, A. R., and Moore, A. T. (2012) High-resolution optical coherence tomography imaging in *KCNV2* retinopathy. *Br. J. Ophthalmol.* **96,** 213–217
31. Thiagalingam, S., McGee, T. L., Weleber, R. G., Sandberg, M. A., Trzupek, K. M., Berson, E. L., and Dryja, T. P. (2007) Novel mutations in the *KCNV2* gene in patients with cone dystrophy and a supernormal rod electroretinogram. *Ophthalmic. Genet.* **28,** 135–142
32. Wissinger, B., Dangel, S., Jägle, H., Hansen, L., Baumann, B., Rudolph, G., Wolf, C., Bonin, M., Koeppen, K., Ladewig, T., Kohl, S., Zrenner, E., and Rosenberg, T. (2008) Cone dystrophy with supernormal rod response is strictly associated with mutations in *KCNV2*. *Invest. Ophthalmol. Vis. Sci.* **49,** 751–757
33. Wissinger, B., Schaich, S., Baumann, B., Bonin, M., Jagle, H., Friedburg, C., Varsanyi, B., Hoyng, C. B., Dollfus, H., Heckenlively, J. R., Rosenberg, T., Rudolph, G., Kellner, U., Salati, R., Plomp, A., De Baere, E., Andrassi-Darida, M., Sauer, A., Wolf, C., Zobor, D., Bernd, A., Leroy, B. P., Enyedi, P., Cremers, F. P., Lorenz, B., Zrenner, E., and Kohl, S. (2011) Large deletions of the *KCNV2* gene are common in patients with cone dystrophy with supernormal rod response. *Hum. Mutat.* **32,** 1298–1406
34. Horton, R. M., Hunt, H. D., Ho, S. N., Pullen, J. K., and Pease, L. R. (1989) Engineering hybrid genes without the use of restriction enzymes: gene splicing by overlap extension. *Gene* **77,** 61–68
35. Schneider, C. A., Rasband, W. S., and Eliceiri, K. W. (2012) National Institutes of Health Image to ImageJ. 25 years of image analysis. *Nature Methods* **9,** 671–675
36. Klemic, K. G., Shieh, C. C., Kirsch, G. E., and Jones, S. W. (1998) Inactivation of Kv2.1 potassium channels. *Biophys. J.* **74,** 1779–1789
37. Bixby, K. A., Nanao, M. H., Shen, N. V., Kreusch, A., Bellamy, H., Pfaffinger, P. J., and Choe, S. (1999) Zn^{2+} binding and molecular determinants of tetramerization in voltage-gated K^+ channels. *Nat. Struct. Biol.* **6,** 38–43
38. Mederos Y Schnitzler, M., Rinné, S., Skrobek, L., Renigunta, V., Schlichthörl, G., Derst, C., Gudermann, T., Daut, J., and Preisig-Müller, R. (2009) Mutation of histidine 105 in the T1 domain of the potassium channel Kv2.1 disrupts heteromerization with Kv6.3 and Kv6.4. *J. Biol. Chem.* **284,** 4695–4704
39. VanDongen, A. M., Frech, G. C., Drewe, J. A., Joho, R. H., and Brown, A. M. (1990) Alteration and restoration of K^+ channel function by deletions at the N and C termini. *Neuron* **5,** 433–443
40. Park, K. S., Mohapatra, D. P., Misonou, H., and Trimmer, J. S. (2006) Graded regulation of the Kv2.1 potassium channel by variable phosphorylation. *Science* **313,** 976–979
41. Park, K. S., Mohapatra, D. P., and Trimmer, J. S. (2007) Proteomic analyses of Kv2.1 channel phosphorylation sites determining cell background specific differences in function. *Channels* **1,** 59–61
42. Ramu, Y., Xu, Y., and Lu, Z. (2006) Enzymatic activation of voltage-gated potassium channels. *Nature* **442,** 696–699
43. Xu, Y., Ramu, Y., and Lu, Z. (2008) Removal of phospho-head groups of membrane lipids immobilizes voltage sensors of K^+ channels. *Nature* **451,** 826–829
44. Schwake, M., Pusch, M., Kharkovets, T., and Jentsch, T. J. (2000) Surface expression and single channel properties of *KCNQ2*/*KCNQ3*. M-type K^+ channels involved in epilepsy. *J. Biol. Chem.* **275,** 13343–13348
45. Es-Salah-Lamoureux, Z., Xiong, P. Y., Goodchild, S. J., Ahern, C. A., and Fedida, D. (2011) Blockade of permeation by potassium but normal gating of the G628S nonconducting hERG channel mutant. *Biophys. J.* **101,** 662–670
46. Bocksteins, E., Labro, A. J., Mayeur, E., Bruyns, T., Timmermans, J. P., Adriaensen, D., and Snyders, D. J. (2009) Conserved negative charges in the N-terminal tetramerization domain mediate efficient assembly of Kv2.1 and Kv2.1/Kv6.4 channels. *J. Biol. Chem.* **284,** 31625–31634
47. Tu, L., Santarelli, V., Sheng, Z., Skach, W., Pain, D., and Deutsch, C. (1996) Voltage-gated K^+ channels contain multiple intersubunit association sites. *J. Biol. Chem.* **271,** 18904–18911
48. Zerangue, N., Jan, Y. N., and Jan, L. Y. (2000) An artificial tetramerization domain restores efficient assembly of functional *Shaker* channels lacking T1. *Proc. Natl. Acad. Sci. U.S.A.* **97,** 3591–3595
49. Chang, Y. F., Imam, J. S., and Wilkinson, M. F. (2007) The nonsense-mediated decay RNA surveillance pathway. *Annu. Rev. Biochem.* **76,** 51–74
50. Beech, D. J., and Barnes, S. (1989) Characterization of a voltage-gated K^+ channel that accelerates the rod response to dim light. *Neuron* **3,** 573–581

51. Cia, D., Bordais, A., Varela, C., Forster, V., Sahel, J. A., Rendon, A., and Picaud, S. (2005) Voltage-gated channels and calcium homeostasis in mammalian rod photoreceptors. *J. Neurophysiol.* **93,** 1468–1475
52. Demontis, G. C., Longoni, B., Barcaro, U., and Cervetto, L. (1999) Properties and functional roles of hyperpolarization-gated currents in guinea-pig retinal rods. *J. Physiol.* **515,** 813–828
53. Werblin, F. S. (1979) Time- and voltage-dependent ionic components of the rod response. *J. Physiol.* **294,** 613–626
54. Yagi, T., and Macleish, P. R. (1994) Ionic conductances of monkey solitary cone inner segments. *J. Neurophysiol.* **71,** 656–665
55. Frings, S., Brüll, N., Dzeja, C., Angele, A., Hagen, V., Kaupp, U. B., and Baumann, A. (1998) Characterization of ether-a-go-go channels present in photoreceptors reveals similarity to I_{Kx}, a K^+ current in rod inner segments. *J. Gen. Physiol.* **111,** 583–599
56. Jentsch, T. J., Hübner, C. A., and Fuhrmann, J. C. (2004) Ion channels. Function unraveled by dysfunction. *Nat. Cell Biol.* **6,** 1039–1047
57. Kullmann, D. M. (2010) Neurological channelopathies. *Annu. Rev. Neurosci.* **33,** 151–172
58. Hejtmancik, J. F., Jiao, X., Li, A., Sergeev, Y. V., Ding, X., Sharma, A. K., Chan, C. C., Medina, I., and Edwards, A. O. (2008) Mutations in *KCNJ13* cause autosomal-dominant snowflake vitreoretinal degeneration. *Am. J. Hum. Genet.* **82,** 174–180